Kinetic Gelation Modeling: Structural Inhomogeneity during Cross-Linking Polymerization

Mei Wen,† L. E. Scriven, and Alon V. McCormick*

Department of Chemical Engineering & Materials Science and Center for Interfacial Engineering, University of Minnesota, Minneapolis, Minnesota 55455

Received February 21, 2001; Revised Manuscript Received December 20, 2002

ABSTRACT: Kinetic gelation models simulate free-radical polymerization on fixed lattices, where propagation and termination reactions are restricted to occur only between nearest neighbors. Here such a model is used with bifunctional sites and with kinetics recast as a Markov process through a stochastic approach. The reaction time is calculated by employing the probability density function and associated Monte Carlo method devised originally by Gillespie. As polymerization proceeds, the evolution of structure is characterized by pair correlation functions of three types—of reacted sites, of doubly reacted sites, and of monomers. These show that as polymerization proceeds, reacted sites and doubly reacted sites come to be distributed more uniformly in space; monomers come to be distributed less uniformly. A higher initiation rate constant, a higher initiator concentration, and a lower propagation rate constant lead to more uniform distribution of reacted sites, of doubly reacted sites, and of monomers. These factors also lead to lower average connectivity between reacted sites. These trends are strongest at low conversions. In contrast, an enhanced primary cyclization leads to less uniform distribution of reacted sites but to more uniform distribution of monomers. It also leads to higher connectivity between reacted sites that are close together but to lower connectivity between reacted sites that are far apart. Finally, at high conversions it leads to a more uniform distribution of doubly reacted sites.

Introduction

Photopolymerization of multifunctional monomers such as diacrylates or dimethacrylates rapidly produces densely cross-linked networks that are useful in applications such as decorative and protective coatings, replication of optical disks and aspherical lenses, and dental restoration.[1−4] One important feature of the development of such networks is spatial inhomogeneity—that is, local variations in conversion so that more highly reacted regions coexist with less highly reacted regions. Because the growth and cross-linking of the network impede the translational and rotational mobilities of reactive functional groups and free radicals, spatial inhomogeneity in cross-link density can affect the overall polymerization kinetics. Moreover, the connectivity of the network that is grown plays a large part in governing material properties such as the modulus.

Qualitatively, the course of events in this sort of network polymerization can easily be anticipated. At low conversions, an active radical at the end of a relatively free chain might more easily attack nearby pendant functional groups than monomeric functional groups. This can lead to enhanced primary cyclization (enhanced beyond what would be expected from the mean-field concentration of functional groups) and beyond that to what are called microgels[5−10]—a distinct region of densely cross-linked network polymer within a less polymerized, largely monomeric background. The formation of microgels should postpone the onset of gelation to higher conversions than predicted by classical gelation theory,[11,12] which ignores cyclization. On the other hand, at high conversions, the apparent reactivity of pendant functional groups should drop gradually as they become shielded with increasing cross-link density.[1,5,9,13] Subsequently, further reaction at the periphery of microgels with still-accessible remaining monomers and less cross-linked polymer fills in the space between the microgels, leading finally to a highly cross-linked polymer network.

It is challenging, though, to quantify and predict these trends and their manipulation with, for instance, light intensity or changing tendency to cyclization (e.g., with monomer flexibility). Because of the varying apparent reactivity of pendant functional groups in the polymerization of multifunctional monomers, it is challenging even to characterize the kinetics of primary cyclization.[7,14−16] Moreover, though various techniques have been used to characterize the structural inhomogeneity (as shown in Table 1), there are no systematic experiments showing quantitatively how different reaction conditions such as initiation rate and cyclization preference affect the structural inhomogeneity. Furthermore, there is still no instrument available to visualize and follow polymer network growth easily to characterize structural inhomogeneity. Luckily, computer simulation of free-radical polymerization on lattices—kinetic gelation modeling—provides a way to improve insight into developing heterogeneities and their effects on the overall kinetics, particularly as one considers manipulating initiation and cyclization rates.

Previous Kinetic Gelation Modeling

A kinetic gelation model simulates free-radical polymerization on a lattice with rules of initiation, propagation, termination, and radical trapping. Reaction is restricted to occur between nearest neighbors. In contrast to random bond percolation where bonds form randomly between any two reactive sites,[17] kinetic gelation is defined as a process in which a kinetic chain is identical with the path of a free radical.[18] Whereas

† Present address: Atofina Chemicals, Inc., 900 First Ave., King of Prussia, PA 19406.

* To whom correspondence should be addressed.

10.1021/ma010308q CCC: $25.00
Published on Web 05/07/2003

Table 1. Techniques of Characterizing Structural Inhomogeneity

technique	response or contrast	relevance
electron spin resonance spectroscopy (ESR)[59,64]	radiation absorption by electrons in magnetic fields	radical concentration and environments
nuclear magnetic resonance spectroscopy (NMR)[5,28,56,65,66]	radiation absorption by nuclei in magnetic fields	rate of spin diffusion, and concentrations of pendant functional groups and monomers and their environments
X-ray scattering[67]	electron density	statistical distribution of polymer size
light scattering[57,68]	refractive index	statistical distribution of polymer size
transmission electron microscopy (TEM)[35]	double bonds stained by OsO_4	size and shape of highly reacted regions
dynamic mechanical analysis (DMA)[69,70]	elastic and loss modulus	relaxation time distribution
positron annihilation lifetime spectroscopy (PALS)[71−73]	lifetime of orthopositronium	free volume distribution
UV−vis photochromic probe technique (PCPT)[74,75]	probe molecules at trans and cis states	free volume distribution

statistical[19,20] and kinetic models[14,15,21−23] that presume reaction occurs uniformly across the entire system are often suitable for lightly cross-linked, relatively homogeneous networks, kinetic gelation modeling is necessary to predict the degrees and types of inhomogeneity that arise in highly cross-linking systems wherein diffusion quickly becomes slow compared to local reaction rates.

Manneville and de Seze[24] were among the first to perform kinetic gelation modeling of free-radical polymerization of multifunctional monomers. They used a simple cubic lattice, each lattice site representing a monomer with either one or two functional groups. All radicals were activated at randomly chosen sites before polymerization; this is the "fast initiation" limit. No physical movement of monomers and polymers was explicitly included (though local thermal motion of sites as necessary for local reaction is implicit). They focused attention on the bond percolation threshold and on the cluster size distribution near the threshold and compared these to expectations from random bond percolation and from classical treelike models.[11,12,25]

In contrast to the "fast initiation" limit, Boots later examined the "slow initiation" limit; only one radical was allowed to be present on the lattice at any time during reaction.[26] He also imposed limits on the maximum kinetic chain length to mimic the effect of changing initiation rate, predicting qualitatively that the distribution of reacted sites should become more uniform as initiation speeds up.

Boots and Pandy[27] also used kinetic gelation modeling, but now at a determined initiation rate. Upon initiation, some monomers were chosen to transform into free radicals. However, the time was gauged by a computational time step, in which a radical and one of its neighbors were chosen to react at random. The actual time for a radical to react might be short early in reaction but long late in reaction as more radicals get trapped and reactive neighbors of active radicals become less. Qualitatively agreeing with experiments of polymerization of styrene and divinylbenzene, the simulation predicted that the apparent reactivity of pendant functional groups is enhanced at low conversions and suppressed at high conversions. Later, Simon et al.[28] simulated initiation somewhat differently by introducing pairs of radicals to sites one unit apart (at the same rate defined by Boots and Pandy). They predicted trends with conversion (but not reaction time) in the amounts of pendant functional groups and of constrained and unconstrained monomers that agreed well with experiments of polymerization of ethylene glycol dimethacrylate.

Bowman and Peppas[29] modeled initiation more realistically by placing initiators on the lattice and intending initiation to follow a first-order rate law. Upon initiation, an initiator became a single radical on the same site. Initiation was assumed to follow first-order kinetics, but it was assumed that at each computational time step each radical has the opportunity to react once if not trapped. This reaction scheme does not necessarily calculate time accurately and so does not necessarily put various reaction rate constants on a consistent footing, but it does serve to illustrate the competition of various rate constants semiquantitatively. This work successfully showed that when initiation was accelerated, the total radical concentration and the maximum reaction rate rose, but the final conversion (approached with the exhaustion of initiators) fell.

The incorporation of additional details into the simulation might certainly give more realistic predictions. Such additional features explored in the literature include simple but explicit motions of monomers and polymers on the lattice[30−33] and multiple occupancy of lattice sites by monomers and even by initiators.[32−35] In general, this body of work shows, though, only minor quantitative changes to the nature of the inhomogeneity and apparent reactivity patterns predicted without these features.

Beyond the scope of this paper, but worth mention here, Anseth and Bowman[34] further examined (with simple motions) the effects of monomer size, initiation rate (defined the same way as described above[29]), amount of solvent, and fraction of difunctional monomer on the apparent pendant functional group reactivity in the copolymerization of mono- and difunctional monomers. They further quantified structural inhomogeneity by recording the probability of finding various types of site pairs next to each other on the lattice.[35] Their examination suggested that microgels should begin to form even at very low conversions. However, the initiation rate did not seem to affect microgel formation. Also, Chiu and Lee[33] and Sun et al.[36] further addressed the cluster size distribution before the percolation threshold (but not local heterogeneity).

Scope

In this paper, we first present a kinetic gelation model that can calculate realistic reaction, or clock, time. We then explore variations of local rate constants sufficiently to reveal the effects of initiation and cyclization on the structure of the evolving network.

The improvement in accounting for reaction time can significantly affect model predictions for two reasons:

(1) unless reaction time is adequately addressed, it is difficult to compare reaction rate constants (particularly those of different order reactions) with experiment, and (2) the structure of the network polymers is innately tied to the balance and sequence of events giving rise to them. In this work, we are able to calculate the real reaction time by recasting polymerization as a Markov process. A stochastic kinetic approach was used, where reaction rate constants were not viewed as reaction rates per unit time per unit volume but as reaction probabilities per unit time.

To solve the stochastic kinetics, we slightly modified and then applied the reaction probability density function and the associated Monte Carlo method that Gillespie first formulated for homogeneous reaction systems.[37] Gillespie's method has been used in simulations of kinetic processes of spatially homogeneous reactions such as complex gas-phase reactions,[38] biochemical reactions,[39] astrochemical reactions,[40] and cross-linking polymerization.[41−44] Also, as Gillespie originally pointed out that this method may be applicable to spatially heterogeneous reaction systems, it has been used in simulations of reactions in molecular crystals,[45] complex catalytic systems,[46] and fractal structures.[47] In this work, the Monte Carlo algorithm developed by Gillespie through defining reaction probability density function was first extended to kinetic gelation modeling. In this way, realistic initiation rates can be simulated; this procedure is described below.

The polymer structure development is quantified by using pair correlation functions. Pair correlation functions give the probability of finding two species of interest at varying distances apart. In this work, the pair correlation functions of reacted sites, of doubly reacted sites, and of unreacted monomers are used. The pair correlation function of reacted sites within the same cluster is also used to gauge the spatial extent of a single molecule.

Particular focus is on trends of inhomogeneity caused by changes in two principal operational variables: the initiation rate (e.g., as controlled in experiments through the light intensity) and primary cyclization enhancement (e.g., as controlled in formulation through the selection of monomer chain flexibility and size). A primary cyclization enhancement factor is defined as the enhancement of the probability that a radical would react to form a primary cycle. The effects of the inhomogeneity trends on polymerization kinetics are presented in the following paper.[48]

For simplicity, explicit movements of monomers and polymers on the lattice were not represented, but local reactive site thermal motions of course were reflected in part in the reaction probabilities, which were themselves proportional to the stochastic reaction rate constants. If movements about, or of, lattice sites were considered explicitly, the associated reaction probabilities would additionally depend on the configurations that were changed by those movements.

Simulation Method

At the start of each simulation, all sites of a simple cubic lattice were occupied randomly either by a monomer with two functional groups or by an initiator molecule. Reaction was allowed only between first-nearest neighbors following rules described shortly. A periodic boundary condition was applied, allowing any molecule on one side of a cube of the lattice to react to form a bond with its counterpart molecule on the opposite side. A rough estimate of the percolation threshold was noted when a cluster came to extend from one side of the lattice to the opposite side, but this threshold does not figure prominently in the trends considered here. (An extrapolation method is available to more accurately represent the percolation threshold of an infinite lattice size,[49] but it is not used here.)

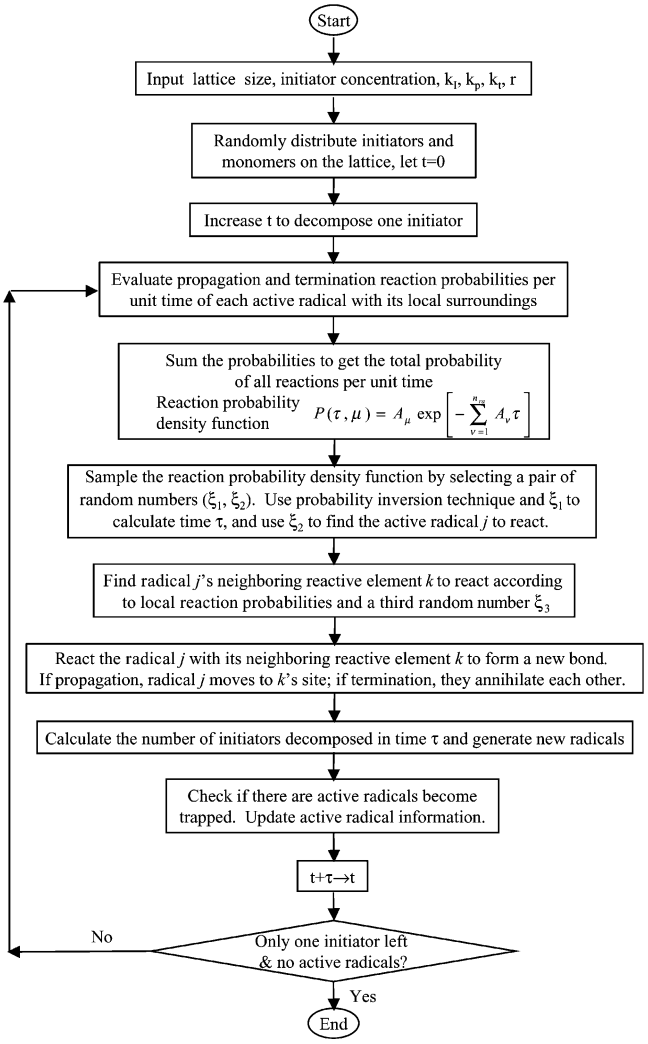

Figure 1. Flowchart of simulation algorithm.

In the following, details of reaction procedures are presented. Both propagation and termination were considered to take place stochastically. Gillespie's reaction probability density function and the associated Monte Carlo method were slightly modified to calculate the waiting time between two consecutive reactions and to choose a pair of reactive sites. A correlation between the stochastic propagation rate constant and the deterministic, experimentally measurable, propagation rate constant was derived to calculate the former. Details of calculating different pair correlation functions for a given network structure are also described below.

The Reaction Procedure. A flowchart of the simulation algorithm is shown in Figure 1.

At the beginning of polymerization, the clock time was advanced to allow one randomly chosen initiator to decompose to free radicals. Here, deterministic kinetics was used for initiation to improve calculation efficiency; it was not necessary to treat initiation stochastically since in almost all cases it was much slower than either propagation or termination (except of course in the

special case $k_I = \infty$, where it is not necessary to simulate initiation rates at all). The time to decompose one initiator was calculated according to the mass-action reaction rate, commonly confirmed in photoinitiated systems

$$\frac{dn_I}{dt} = -k_I n_I \tag{1}$$

where n_I is the number of initiators and k_I is the initiation rate constant. (For example, the clock time required to allow the first initiator to decompose is $1/(k_I n_{I0})$, where n_{I0} is the initial number of initiators on the lattice.) The initiator generated two primary radicals, each presumed to have the same reactivity.[50] The two primary radicals then underwent propagation reactions (this step is presumed instantaneous) with two neighboring monomers to form chain initiating radicals for further reaction. (The initiator site remained occupied by the residue of the initiator, which could react no more.) Once the initial initiation was finished, the system was ready to go into the reaction loop (shown in Figure 1) as described below.

First, for each active radical (not trapped yet), its neighboring functional groups and radicals were counted. The probability that the ith active radical reacts with one of its neighbors in the next time interval δt was calculated as

$$A_i \delta t = [k_p(N_{M1})_i + rk_p(N_{M2})_i + k_t(N_R)_i]\delta t \tag{2}$$

where A_i is the reaction probability per unit time of the ith active radical, k_p is the stochastic propagation rate constant (probability of propagation per unit time), r is a primary cyclization enhancement factor (i.e., the product of r and k_p is the stochastic primary cyclization rate constant), k_t is the stochastic termination rate constant, $(N_{M1})_i$ is the number of neighboring functional groups that cannot form primary cycles with the ith active radical, $(N_{M2})_i$ is the number of neighboring functional groups that can, and $(N_R)_i$ is the number of radicals neighboring the ith active radical.

A waiting time τ before the actual reaction took place was then calculated, and the reacting radical was chosen according to the following algorithm that Gillespie developed.[37] Here, a probability density function, $P(\tau,\mu)$, was defined as the probability at time t that the next reaction in the system volume V would be performed by the μth radical and would occur in the time interval $(t + \tau, t + \tau + d\tau)$. It is a joint probability density function in the space of the continuous variable, of the waiting time τ ($0 \le \tau < \infty$), and of the discrete variable μ ($\mu = 1, 2, ..., n_{ra}$), where n_{ra} is the total number of active radicals. Here, only slightly modifying Gillespie's treatment of examining each type of reactions, we instead examined each active radical. (Because of the potentially heterogeneous nature of reactions on a lattice, each radical may have a different assortment of opportunities.) The following relation he derived was still valid.

$$P(\tau,\mu) = A_\mu \exp[-\sum_{\nu=1}^{n_{ra}} A_\nu \tau] \tag{3}$$

A Monte Carlo technique was used to simulate the stochastic process described by $P(\tau,\mu)$ in eq 3. A pair of random numbers (ξ_1,ξ_2) was generated to calculate the waiting time τ by

$$\tau = -\frac{\ln(\xi_1)}{A_{tot}} \tag{4}$$

where

$$A_{tot} = \sum_{i=1}^{n_{ra}} A_i$$

and to choose the radical that was going to react next, named radical j, by

$$\frac{\sum_{i=1}^{j-1} A_i}{A_{tot}} \le \xi_2 < \frac{\sum_{i=1}^{j} A_i}{A_{tot}} \tag{5}$$

The probability density function does not specify which neighboring reactive element is going to react with the chosen radical, so a third random number ξ_3 was generated to choose a neighboring functional group or free radical, named element k, according to the reaction probabilities involved

$$\frac{\sum_{l=1}^{k-1} a_{jl}}{A_j} \le \xi_3 < \frac{\sum_{l=1}^{k} a_{jl}}{A_j} \tag{6}$$

where a_{jl} is the stochastic reaction rate constant (k_p, rk_p, or k_t) between radical j and its lth neighboring reactive element. (A similar approach, called cascade classification, can be found in Monte Carlo simulation of diffusion-limited reaction on a fractal lattice.[47])

The reaction between the radical j and its neighboring reactive element k then took place. If propagation occurred, a new bond formed between the two lattice sites, and radical j moved to the reacting neighbor site. If termination occurred, radical j and k annihilated each other and also formed a new bond there (termination was considered to be combination only).

After the chosen reaction occurred, initiation was checked to examine whether there were new free radicals generated during the waiting time. The probable number of initiators that were going to decompose since the last initiation, Δn_I, was calculated by

$$\Delta n_I = n_{I0}[\exp(-k_I t_1) - \exp(-k_I t_2)] \tag{7}$$

where t_1 is the time when the last initiation occurred and t_2 is equal to the current time t plus the waiting time τ. The value of t_1 was not necessarily equal to t, e.g., if the reaction loop before the just finished one was too fast to decompose an initiator. If $\Delta n_I \ge 1$, then t_1 was updated by t_2 for future calculation, but if $\Delta n_I < 1$, t_1 did not change and no new initiators were decomposed. When there were new initiators decomposed, they were chosen randomly from the remaining ones on the lattice.

Again each initiator generated two primary radicals upon decomposition. The two primary radicals required at least two reactive neighbors to either propagate or terminate (again, this step is presumed instantaneous); otherwise, the two primary radicals terminated each other, recombining into an inactive molecule occupying the site of the original initiator. The newly generated

active radicals then participated reactions starting from the beginning of a new loop.

At the end of the reaction loop, all current active radicals were checked to see whether any of them had become trapped (i.e., no reactive neighbors remained available). Then the total elapsed clock time (or reaction time t) was augmented by the waiting time τ.

Then the system started a new reaction loop. If it happened that before a new reaction loop started, no active radical existed (e.g., no radical could react because all radicals had become trapped), then reaction time t was increased as required to allow one initiator to decompose (to allow t_2 big enough to decompose one initiator in eq 7). In this way, computation effort was not wasted on uneventful simulation steps, but the reaction time remained accurate.

Simulation was continued until all initiators on the lattice except the last one were exhausted, and there were no more active radicals present. (One initiator was left because eq 1 would require an infinitely long time to decompose all initiators.)

Propagation Rate Constant. The stochastic propagation rate constant k_p (1/s) used here of course differs from but is intimately related to the conventional, deterministic propagation rate constant k_p' (L/(mol s)). The latter is defined by the propagation rate R_p (mol/(L s)), the functional group concentration $[M_{tot}]$ (mol/L), and the total concentration of radicals (including both active and trapped) $[R_{tot}]$ (mol/L).

$$R_p = k_p'[R_{tot}][M_{tot}] \tag{8}$$

When free radical cross-linking polymerization is severely diffusion-controlled, a good deterministic kinetic model must allow k_p' to change as a function of functional group concentration.[22] Thus, it is essentially an apparent deterministic propagation rate constant. However, in the kinetic gelation model described here, we can presume the stochastic propagation rate constant (k_p), which is local propagation probability per unit time, does not change. Regardless of which modeling method to use, the propagation rates should be equal. On the basis of this principle, a correlation between k_p' and k_p can be found as derived below.

The total propagation probability inside the system volume V, $(A_p)_{tot}\delta t$, is the sum of the propagation probability of every active radical (each of which can be calculated by the first two terms in eq 2):

$$(A_p)_{tot}\delta t = [k_p\sum_{i=1}^{n_{ra}}(N_{M1})_i + rk_p\sum_{i=1}^{n_{ra}}(N_{M2})_i]\delta t \tag{9}$$

This can be simplified to

$$(A_p)_{tot}\delta t = k_p\overline{(N_M)_{rad}}n_r\delta t \tag{10}$$

where n_r is the total number of radicals (including active and trapped) and $\overline{(N_M)_{rad}}$ is the apparent average number of functional groups neighboring each radical (whether active or trapped), defined as

$$\overline{(N_M)_{rad}} \equiv \frac{\sum_{i=1}^{n_{ra}}(N_{M1})_i + r\sum_{i=1}^{n_{ra}}(N_{M2})_i}{n_r} \tag{11}$$

In eq 11, the number of trapped radicals is absent from the numerator because they have no neighboring functional groups. As illustrated by Gillespie,[37] the propagation rate R_p here is the total propagation probability per unit time divided by the system volume V and Avogadro's number N_A after taking an average (denoted as $\langle ... \rangle$) over an ensemble of stochastically identical systems.

$$R_p \equiv \left\langle \frac{(A_p)_{tot}\delta t}{VN_A\delta t} \right\rangle = k_p\frac{\langle\overline{(N_M)_{rad}}n_r\rangle}{VN_A} \tag{12}$$

In the deterministic formulation eq 8, $[R_{tot}] = \langle n_r\rangle/N_AV$ and $[M_{tot}] = \langle n_m\rangle/N_AV$, where n_m is the total number of functional groups. Furthermore, since there is no correlation between n_r and $\overline{(N_M)_{rad}}$ when $n_r > 0$, the assumption is made: $\langle n_r\overline{(N_M)_{rad}}\rangle = \langle n_r\rangle\langle\overline{(N_M)_{rad}}\rangle$. Substituting these relations into eq 8 and comparing the propagation rate with that in eq 12 give

$$k_p' = \frac{\langle\overline{(N_M)_{rad}}\rangle}{[M_{tot}]}k_p \tag{13}$$

Equation 13 demonstrates that, at a given conversion of functional groups (where $[M_{tot}]$ is fixed), the deterministic propagation rate constant k_p' is related to the stochastic propagation rate constant k_p by a factor determined by the apparent average number of functional groups neighboring each radical $\langle\overline{(N_M)_{rad}}\rangle$. Equation 13 is also useful to extract the value of k_p from experimentally measured k_p' at the beginning of polymerization, where diffusion limitation has not started yet. A similar correlation can be found in molecular dynamics simulation of a single polymer chain growth where propagation is only allowed within a certain encounter distance between a free radical and functional groups.[51]

Pair Correlation Function. The pair correlation function of reacted sites (i.e., at least one functional group in the monomer has reacted), $g_{rs}(R)$, was calculated by choosing a particular reacted site (to be called the center site) and building a set of concentric spheres with a unit increase in radius around the center site. The number of reacted sites within the unit shell at distance R from the center site, $N_{rs}(R, R + dR)$, was counted, and then this number was normalized by the total number of reacted sites in the shell according to the average density of reacted sites, ρ_{rs}:

$$g_{rs}(R) = \frac{N_{rs}(R, R + dR)}{N_{ls}(R, R + dR)\rho_{rs}} \tag{14}$$

where $N_{ls}(R, R + dR)$ is the total number of lattice sites in the unit shell at distance R from the center site and dR is one lattice unit length. ρ_{rs} equals the total number of reacted sites on the lattice divided by the total number of lattice sites. Periodic boundary conditions were implemented by using mirror images of the system. The average value of $g_{rs}(R)$ was obtained by repeating this process, choosing as the center site each reacted site on the lattice.

The *restricted* pair correlation function of reacted sites *within the same cluster* (which can include the percolating network), $g_{cluster}(R)$, was calculated by counting the number of reacted sites connected to the center site and within the unit shell at distance R from the center site, $N_{cluster}(R, R + dR)$. To compare $g_{cluster}(R)$ with $g_{rs}(R)$,

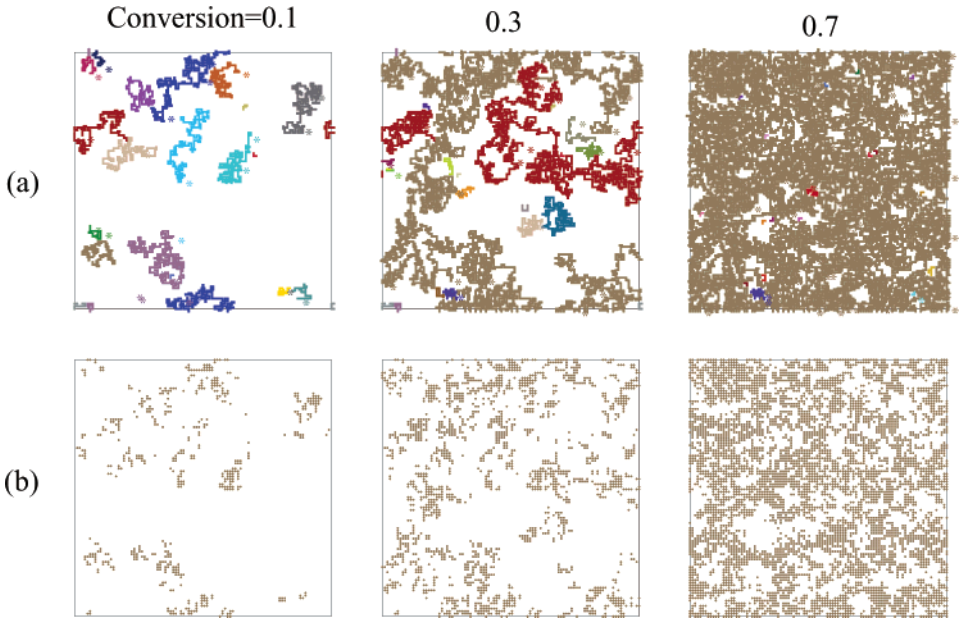

Figure 2. Snapshots of two-dimensional square lattice (100 × 100) simulations (initiator % = 5%) at 0.1, 0.3, and 0.7 conversion. (a) Snapshots of clusters (identified by different colors). Here only bonds and radicals are shown. A thin line was used to represent one bond formed between two lattice sites; a thicker line represents two bonds formed; and the thickest line represents three bonds formed. Each radical is represented by an asterisk. (b) Snapshots of doubly reacted sites (indicated by dots).

the same normalization was used.

$$g_{\text{cluster}}(R) = \frac{N_{\text{cluster}}(R, R + \mathrm{d}R)}{N_{\text{ls}}(R, R + \mathrm{d}R)\rho_{\text{rs}}} \tag{15}$$

Again, the average value of $g_{\text{cluster}}(R)$ was obtained by repeating this process, choosing as the center site each of the reacted sites on the lattice.

The pair correlation function of doubly reacted sites (i.e., both functional groups in a monomer have reacted), $g_{\text{dbr}}(R)$, was calculated by counting the number of doubly reacted sites within the unit shell at distance R from the center doubly reacted site, $N_{\text{dbr}}(R, R + \mathrm{d}R)$. It was then normalized by the total number of doubly reacted sites in the shell according to the average density of doubly reacted sites, ρ_{dbr}:

$$g_{\text{dbr}}(R) = \frac{N_{\text{dbr}}(R, R + \mathrm{d}R)}{N_{\text{ls}}(R, R + \mathrm{d}R)\rho_{\text{dbr}}} \tag{16}$$

The average value of $g_{\text{dbr}}(R)$ was obtained by repeating this process, choosing as the center site each of the doubly reacted monomer site on the lattice.

The pair correlation function of monomer sites (unreacted), $g_{\text{m}}(R)$, was calculated by counting the number of monomers within the unit shell at distance R from the center monomer site, $N_{\text{m}}(R, R + \mathrm{d}R)$. It was then normalized by the total number of monomer sites in the shell according to the average density of the monomer sites, ρ_{m}:

$$g_{\text{m}}(R) = \frac{N_{\text{m}}(R, R + \mathrm{d}R)}{N_{\text{ls}}(R, R + \mathrm{d}R)\rho_{\text{m}}} \tag{17}$$

The average value of $g_{\text{m}}(R)$ was obtained by repeating this process, choosing as the center site each of unreacted monomer site on the lattice.

Modeling Parameters. Typical simulations were run on a 40 × 40 × 40 lattice. This lattice size was found to be large enough so that further increases no longer qualitatively affected the results and trends described below. A set of base-case parameters were set as 1% initiator concentration (the ratio of the initial number of initiators to the total number of lattice sites), $k_{\text{I}} = 1$ 1/s, $k_{\text{p}} = 10^3$ 1/s, $k_{\text{t}} = 10^7$ 1/s, and $r = 1$. The stochastic propagation rate constant k_{p} was estimated (see eq 13) according to the experimental initial propagation rate constants of acrylates $k_{\text{p}}' \approx 1000$ L/(mol s),[52] initial apparent average number of functional groups neighboring each radical $\langle(\overline{N_{\text{M}}})_{\text{rad}}\rangle = 10$, and the initial functional group concentration $[\text{M}_{\text{tot}}] \approx 10$ mol/L (such as in diacrylates). The stochastic termination rate constant k_{t} was chosen to be consistent with the experimental ratio of the propagation rate constant to the termination rate constant ($k_{\text{t}}' \approx 10^7$ L/(mol s))[52] at the beginning of reaction. The initiation rate constants were varied from 0.1 to 10 1/s. They are equivalent to a range of UV intensity from 0.22 to 22 W/cm^2 if the photoinitiator used has an extinction coefficient of 150 L/(mol cm) at an applied wavelength of 365 nm; these values are typical in industrial radiation curing of coatings.[2,4]

In the calculation of the pair correlation functions, the average of five realizations was reported. In each realization, the seed of the random number generator (Park and Miller's minimal standard generator[53]) was changed. In the figures below, range bars show plus or minus one standard deviation of the five realizations. Though some pairs of range bars overlap, apparent trends are shown by examining at least several data points (which do not all overlap each other).

The effects of initiation rate constant and primary cyclization rate constant on the pair correlation functions $g_{\text{rs}}(R)$, $g_{\text{cluster}}(R)$, $g_{\text{m}}(R)$, and $g_{\text{dbr}}(R)$ are discussed below.

Results and Discussion

The snapshots generated at different stages of a small two-dimensional square lattice simulation (see Figure 2) serve to preview the qualitative features of polymer

Table 2. Conversion of Functional Groups at Percolation Threshold, x_c[a]

k_I	r	x_c	k_I	r	x_c
0.1	1	0.014 ± 0.006			
1	1	0.026 ± 0.005	1	3	0.036 ± 0.011
10	1	0.05 ± 0.007	1	9	0.053 ± 0.010

[a] The plus or minus range is one standard deviation of x_c for 20 runs.

and network growth on a lattice that we will examine quantitatively below.

Figure 2a shows that as polymerization proceeds, more monomer sites convert to reacted sites, and clusters form around initiating free radicals. Further reaction not only generates new clusters but also connects clusters together, forming a percolating network. Beyond a certain conversion, the system has become one big percolating network with few small clusters and monomer pools or pockets embedded. (The large percolating network, of course, may still be clumpy, made of formerly distinct clusters tied together.) In the reaction process, the spatial distribution of the reacted sites becomes more uniform, but that of the monomer sites becomes less uniform. Moreover, Figure 2b shows that as more doubly reacted sites are generated—that is, as the system becomes denser and more highly cross-linked—the spatial distribution of the doubly reacted sites becomes more uniform.

In the following, the structure trends in three-dimensional simulation are quantified by the pair correlation functions, $g_{rs}(R)$, $g_{cluster}(R)$, $g_m(R)$, and $g_{dbr}(R)$. In particular, the effects of initiation rate constant and primary cyclization rate constant on the structure trends are examined. In all of the three-dimensional simulations below, the percolation threshold remained below 0.1 conversion of functional groups (as shown in Table 2). Though earlier researchers focused on the percolation threshold, it was found that the pair correlation functions discussed here show local structure changes much more clearly. In no case does the local structure as shown by pair correlation functions show any marked change upon passing through the percolation threshold.

Effect of Initiation Rate Constant. Figure 3 shows the pair correlation function of reacted sites, $g_{rs}(R)$, at different stages of reaction. $g_{rs}(R)$ is highest at $R = 1$, gradually decaying to unity at long distance. That $g_{rs}(R)$ is higher than unity at short distance indicates that the reacted sites are distributed nonuniformly in space, tending to form clusters associated with small polymers. As polymerization proceeds, the value of $g_{rs}(R = 1)$ drops only because more monomer sites have converted to reacted sites, leading to a more uniform distribution of reacted sites in space. Consistent with the trends observed by Anseth et al.,[35] the value of $g_{rs}(R = 1)$ can be used as a measure of how heterogeneous the distribution of the reacted sites is. Further, though, it appears that the rate of decay of $g_{rs}(R)$ with R might supply an additional measure of heterogeneity.

As the initiation rate constant is raised, $g_{rs}(R)$ drops at short R; this effect is most apparent at low conversions. One may infer that increasing the initiation rate constant causes a more homogeneous distribution of reacted sites, particularly when the system has only achieved low conversion. This results from the birth of more numerous polymer chains (at a given conversion) with the faster generation of free radicals. (The effect of initiation rate constant fades at high conversions, though, simply because reacted sites must become more uniformly distributed when more sites have reacted.)

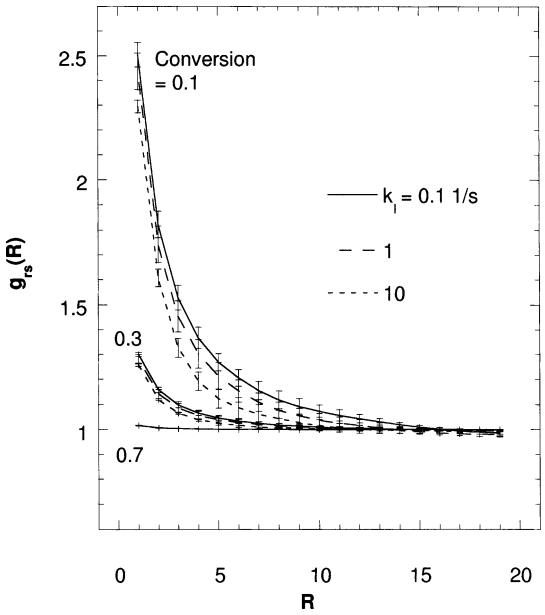

Figure 3. Effect of initiation rate constant k_I on the pair correlation function of reacted sites, $g_{rs}(R)$, at different conversions: 0.1, 0.3, and 0.7. Range bars indicate plus or minus one standard deviation.

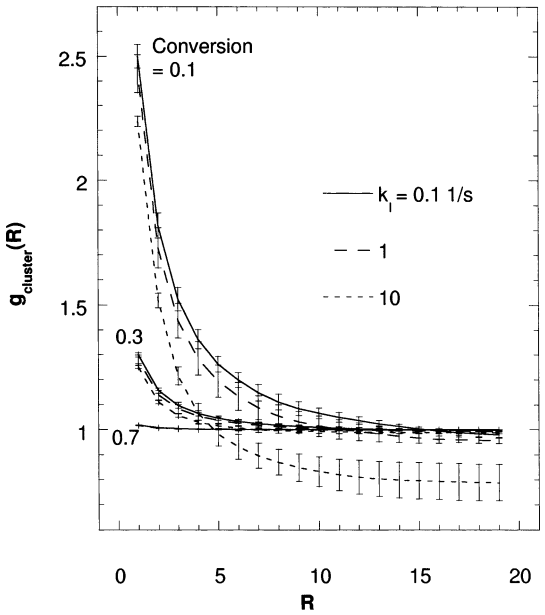

Figure 4. Effect of initiation rate constant k_I on the restricted pair correlation function of reacted sites within the same cluster, $g_{cluster}$, at different conversions: 0.1, 0.3, and 0.7. Range bars indicate plus or minus one standard deviation.

Figure 4 shows the *restricted* pair correlation function of reacted sites *within the same cluster*, $g_{cluster}(R)$; this should provide a more sensitive measure of structure than $g_{rs}(R)$, because $g_{cluster}(R)$ indicates the connectivity between the reacted sites through bonds. Similar to $g_{rs}(R)$, $g_{cluster}(R)$ suggests that reacted sites have higher connectivity in shorter distance. Because the same normalization (the average density of reacted sites) is used, though, $g_{cluster}(R)$ is smaller than $g_{rs}(R)$ and can even fall to values below unity at long R. The R value at the crossover is a characteristic size of highly reacted regions—clusters or former clusters that are now linked

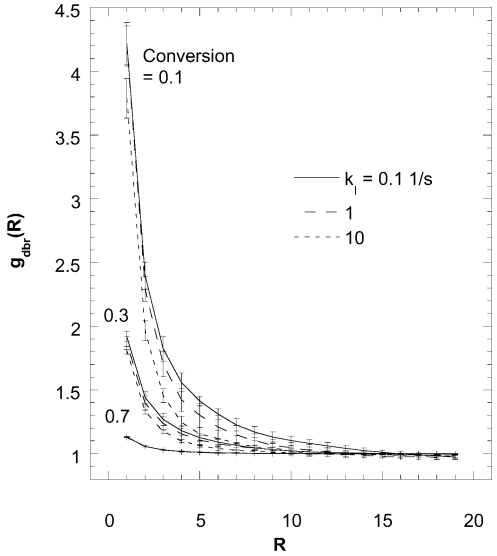

Figure 5. Effect of initiation rate constant k_I on the pair correlation function of doubly reacted sites, $g_{dbr}(R)$, at different conversions: 0.1, 0.3, and 0.7. Range bars indicate plus or minus one standard deviation.

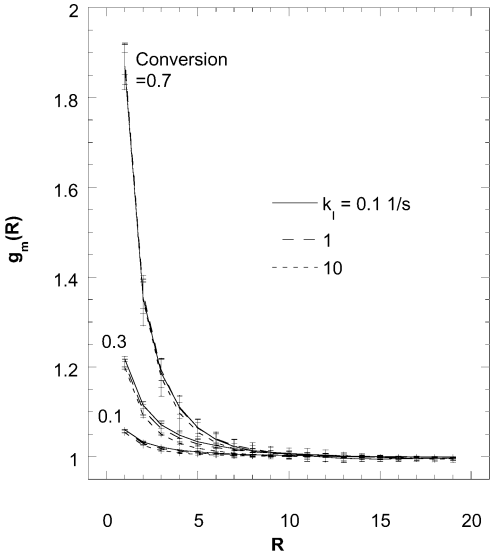

Figure 6. Effect of initiation rate constant k_I on the pair correlation function of monomer sites, $g_m(R)$, at different conversions: 0.1, 0.3, and 0.7. Range bars indicate plus or minus one standard deviation.

together in a large cluster. The difference between $g_{cluster}(R)$ and $g_{rs}(R)$ increases with R because fewer reacted sites are connected to the center reacted site; the bigger this difference, the poorer the connectivity. As polymerization proceeds, more and more clusters connect together and to the percolating network.

Increasing the initiation rate constant lowers $g_{cluster}(R)$ at all R, indicating lower connectivity between reacted sites. The higher the initiation rate constant, the larger the difference between $g_{cluster}(R)$ and $g_{rs}(R)$, again suggesting lower connectivity of reacted sites. (As polymerization proceeds, more reacted sites are connected together, so this difference becomes smaller.)

Figure 5 shows the pair correlation function of doubly reacted sites, $g_{dbr}(R)$, which contribute to the formation of primary cycles, secondary cycles, and cross-links.[54] $g_{dbr}(R)$ shows a trend similar to $g_{rs}(R)$; however, $g_{dbr}(R)$ at short R is much larger than $g_{rs}(R)$, indicating less uniform distribution of doubly reacted sites than of any reacted sites. This owes mainly to the localized formation of cycles in the vicinity of initiators, tending to form localized regions of cyclization and cross-linking. This sort of pattern has previously been observed in the simulation of copolymerization of monofunctional and difunctional monomers in a solvent-born system.[55] (At high conversions, though, more doubly reacted sites are formed, so the distribution of the doubly reacted sites becomes more uniform and the spatial correlation becomes weaker.)

As the initiation rate constant is raised, $g_{dbr}(R)$ drops at short R, meaning that doubly reacted sites become more uniformly distributed; this trend is most apparent at low conversions. This is consistent with the more homogeneous distribution of all reacted sites suggested by $g_{rs}(R)$. (At high conversions, more and more monomer sites have reacted twice, and the distribution of the doubly reacted sites is more uniform, so the effect of initiation rate constant diminishes.)

Figure 6 shows the pair correlation function of unreacted monomer sites, $g_m(R)$, which can indicate whether there are pools of unreacted monomer. $g_m(R)$ is highest at $R = 1$, and then it gradually decays to unity at long R; this indicates that monomer sites are distributed nonuniformly in space, tending to form monomer pools. In contrast to the other correlation functions, $g_m(R)$ at small R rises as polymerization proceeds; liquid monomer pools tend to form more distinctly later in reaction, as there come to be regions where free radicals find no access.

As the initiation rate constant is raised, $g_m(R)$ drops at short R; this trend is most apparent at low conversions. With faster initiation (and more populous radicals), there is less of a tendency to find monomer pools.

In summary, the simulations show that faster initiation leads to a more homogeneous network at a given conversion. However, it also leads to poorer connectivity between sites.

The prediction that the network becomes more uniform at higher conversions (at any initiation rate) agrees with previous work. In the cross-polarization magic angle spinning (CPMAS) ^{13}C studies of copolymerization of triacrylate with di(meth)acrylate, it was found that the rate of spin diffusion rises as conversion of double bonds gets higher, indicating that polymer network becomes more homogeneous as polymerization proceeds.[56] The formation of more homogeneous structure by connecting more clusters or microgels together further agrees with Dusek's model of network formation. In his model, the intercluster space is gradually filled in with newly formed polymer chains from radicals reacting with pendant functional groups on the periphery of existing clusters or microgels, and the density fluctuations become smaller.[6−8]

The prediction that faster initiation should produce a more uniform network (at a given conversion) is consistent with several previous, more qualitative, simulation results. It is consistent with Boots' prediction of spatial distribution of reacted sites as the maximum kinetic chain length is shortened[26] and with the polymer snapshots predicted by Anseth and Bowman[35] (though no clear trend was observed in their probability of finding adjacent reacted site pairs). We have found no clear experimental data showing how the network homogeneity is affected by the initiation rate constant.

Finally, the predicted poorer connectivity of reacted sites when the initiation rate constant is raised agrees

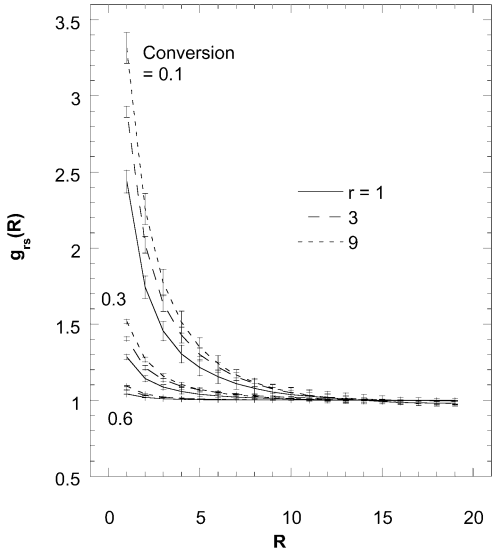

Figure 7. Effect of primary cyclization enhancement factor r on the pair correlation function of reacted sites, $g_{rs}(R)$, at different conversions: 0.1, 0.3, and 0.6. Range bars indicate plus or minus one standard deviation.

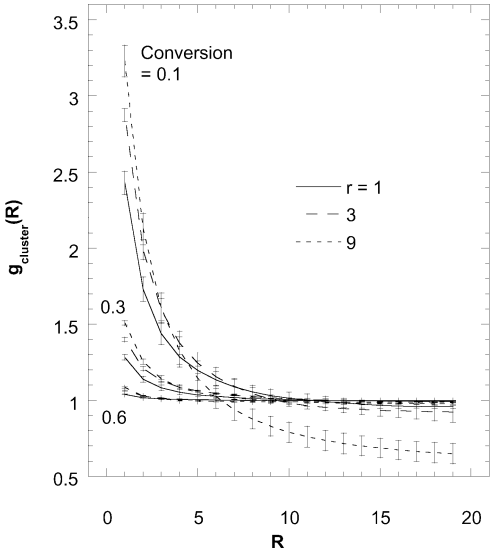

Figure 8. Effect of primary cyclization enhancement factor r on the restricted pair correlation function of reacted sites within the same cluster, $g_{cluster}(R)$, at different conversions: 0.1, 0.3, and 0.6. Range bars indicate plus or minus one standard deviation.

with light scattering experiment result that smaller polymer clusters are formed at a higher temperature in thermoinitiated polymerization of ethylene glycol dimethacrylate.[57]

Raising the initiator concentration (results not shown here) leads to essentially the same trend as the initiation rate constant is raised. However, it should be noted that the coater can ordinarily easily vary the light intensity (and so the initiation rate constant) over a wider range than the photoinitiator concentration.

Dropping the propagation rate constant by 3 orders of magnitude (results not shown here) produces similar effects as raising the initiation rate constant. Because the termination rate constant $k_t = 10^7$ 1/s and the propagation rate constant $k_p = 10^3$ 1/s, the change of k_p even by 3 orders of magnitude from 10^2 to 10^4 1/s does not affect much the relative probability of propagation to termination. Therefore, at a given incremental of conversion dx (where x denotes conversion), the time spent dt is inversely proportional to k_p: the faster the propagation, the shorter the time needed. Consequently, less initiators are decomposed and less free radicals are generated in dt. This is exactly the same as the initiation rate constant k_I is lowered (see eq 1). Therefore, increasing the propagation rate constant gives the same trend of network structures at a given conversion as the initiation rate constant is lowered.

Effect of Primary Cyclization Enhancement. Figure 7 shows the pair correlation function of reacted sites, $g_{rs}(R)$, as primary cyclization is enhanced (as r increases). $g_{rs}(R)$ increases at short R, indicating a less uniform distribution of reacted sites. This effect does not diminish at high conversions as the effect of the initiation rate did. Here, though, heterogeneity arises for new reason; enhanced primary cyclization causes the formation of highly cyclized regions, with the more reacted sites localized in the vicinity of initiating free radicals.

Figure 8 shows that enhanced primary cyclization increases $g_{cluster}(R)$ at short R and lowers $g_{cluster}(R)$ at long R. The more enhanced primary cyclization is, the larger the difference between $g_{cluster}(R)$ and $g_{rs}(R)$, particularly at low conversions.

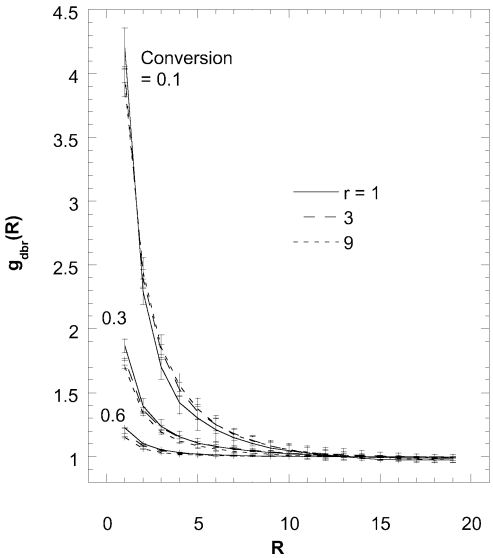

Figure 9. Effect of primary cyclization enhancement factor r on the pair correlation function of doubly reacted sites, $g_{dbr}(R)$, at different conversions: 0.1, 0.3, and 0.6. Range bars indicate plus or minus one standard deviation.

Figure 9 shows that enhanced primary cyclization does not affect the distribution of doubly reacted sites $g_{dbr}(R)$ at low conversions, though it causes a more uniform distribution of doubly reacted sites at high conversions. Moreover, Figure 10 shows that enhanced primary cyclization causes a more homogeneous distribution of monomer sites. It appears that the reacted sites become more highly connected at short range but less highly connected at long range when primary cyclization is enhanced. This leaves more monomer sites unreacted.

In summary, enhancing primary cyclization tends to decrease the homogeneity of the network formed, and it tends to produce highly cyclized clusters. These trends are consistent with previous suggestions[1,7,34,58−60] that a heterogeneous structure is formed in the free radical cross-linking polymerization because of cyclization.

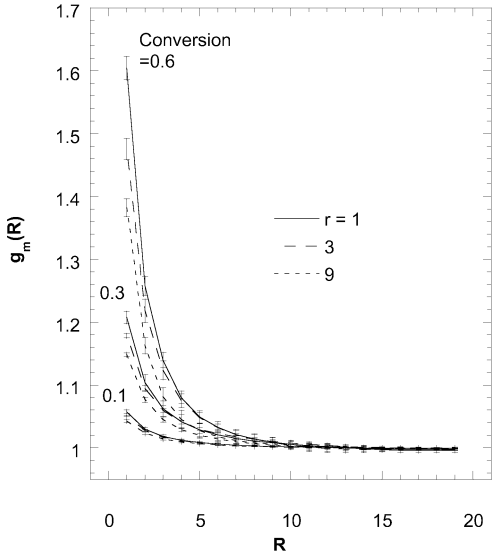

Figure 10. Effect of primary cyclization enhancement factor r on the pair correlation function of monomer sites, $g_m(R)$, at different conversions: 0.1, 0.3, and 0.6. Range bars indicate plus or minus one standard deviation.

It has been shown that primary cyclization can be enhanced when the chain length between two double bonds gets shorter,[56,60] and it is generally thought that this enhancement is caused both by monomer chain flexibility and by spatial proximity of reactive groups. Accordingly, recent work has assumed that small difunctional monomers should exhibit enhanced cyclization.[16,34] The current model suggests that this may lead to a more heterogeneous network structure.

Conclusions

Unlike previous realizations of kinetic gelation models, polymerization kinetics is recast as a Markov process through a stochastic approach. We are able to calculate real reaction time by modifying and employing the probability density function and the associated Monte Carlo method devised originally by Gillespie to reactions on a lattice. Moreover, the structure evolution during the polymerization of difunctional monomers is characterized with pair correlation functions of reacted sites, doubly reacted sites, and monomer sites. The general trends reported here should be relevant to the behavior of higher functionality monomers as well.

In all cases, as polymerization proceeds, the spatial distributions of reacted sites and of doubly reacted sites become more uniform, but the spatial distribution of monomer sites becomes less uniform. The homogenization of the network as polymerization proceeds has been confirmed by experiment.[7,8,56]

A higher initiation rate constant, a higher initiator concentration, and a lower propagation rate constant have a similar effect on the structure development, so it is useful to refer to the initiation ratio $k_I[I]_0/k_p[M_{tot}]_0$ (where $[I]_0$ is the initial initiator concentration and $[M_{tot}]_0$ is the initial functional group concentration). Increasing the initiation ratio leads to a lower connectivity between reacted sites. Particularly at low conversions, this leads to more uniform distributions of reacted sites, doubly reacted sites, and unreacted monomer sites—a more uniform network. This is consistent with previous observations,[26,35] but the trend becomes clearer in this set of simulations and with the use of pair correlation functions.

Enhanced primary cyclization leads to higher connectivity between reacted sites that are close together, but a lower connectivity between reacted sites that are far apart. It leads to less uniform distribution of reacted sites, but a more uniform distribution of monomers. Enhanced cyclization leads to a more heterogeneous network.

The studies presented support the following strategy if one wishes to produce homogeneous cross-linking polymerization: increase the initiation rate (through either UV intensity or initiator concentration) relative to propagation and ensure that formulators provide multifunctional monomers that are not likely to undergo primary cyclization, such as those with long and relatively inflexible chain lengths between functional groups.[61] Conversely, if one wishes to produce particles, provide multifunctional monomers with a molecular architecture prone to produce primary cyclization and under high dilution. Such strategies have been applied to study and to make microgel particles.[7,10,62,63]

Acknowledgment. We acknowledge support from the Center for Interfacial Engineering, a NSF Engineering Research Center at the University of Minnesota, through its Coating Process Fundamentals Program.

References and Notes

(1) Kloosterboer, J. G. *Adv. Polym. Sci.* **1988**, *84*, 1−66.
(2) Pappas, S. P. *Radiation Curing: Science and Technology*; Plenum: New York, 1992.
(3) Decker, C.; Zahouily, K. *Polym. Mater. Sci. Eng.* **1993**, *68*, 70−71.
(4) Fouassier, J.-P., Rabek, J. F., Eds.; *Radiation Curing in Polymer Science and Technology;* Elsevier Applied Science: London, 1993; Vol. 4.
(5) Dusek, K.; Spevacek, J. *Polymer* **1980**, *21*, 750−756.
(6) Dusek, K.; Galina, H.; Mikes, J. *Polym. Bull. (Berlin)* **1980**, *3*, 19−25.
(7) Dusek, K. In *Developments in Polymerisation-3*; Haward, R. N., Ed.; Applied Science: London, 1982; Chapter 4, pp 143−206.
(8) Dusek, K. *Angew. Makromol. Chem.* **1996**, *240*, 1−15.
(9) Galina, H.; Dusek, K.; Tuzar, Z.; Bohdanecky, M.; Stokr, J. *Eur. Polym. J.* **1980**, *16*, 1043−1046.
(10) Funke, W. *Br. Polym. J.* **1989**, *21*, 107−115.
(11) Flory, P. J. *J. Am. Chem. Soc.* **1941**, *63*, 3083−3090.
(12) Stockmayer, W. H. *J. Chem. Phys.* **1943**, *11*, 45−55.
(13) Minnema, L.; Staverman, A. J. *J. Polym. Sci.* **1958**, *29*, 281.
(14) Tobita, H.; Hamielec, A. *Makromol. Chem., Macromol. Symp.* **1988**, *20/21*, 501−543.
(15) Tobita, H.; Hamielec, A. *Macromolecules* **1989**, *22*, 3098−3105.
(16) Elliott, J. E.; Bowman, C. N. *Macromolecules* **1999**, *32*, 8621−8628.
(17) Stauffer, D.; Aharony, A. *Introduction to Percolation Theory*, 2nd ed.; Taylor & Francis: London, 1992.
(18) Sahimi, M. *Applications of Percolation Theory*; Taylor & Francis: Bristol, PA, 1994.
(19) Dotson, N.; Galvan, R.; Macosko, C. W. *Macromolecules* **1988**, *21*, 2560−2568.
(20) Scranton, A.; Peppas, N. *J. Polym. Sci., Polym. Chem.* **1990**, *28*, 39−57.
(21) Mikos, A.; Takoudis, C.; Peppas, N. A. *Macromolecules* **1986**, *19*, 2174−2182.
(22) Bowman, C. N.; Peppas, N. A. *Macromolecules* **1991**, *24*, 1914−1920.
(23) Kurdikar, D. L.; Peppas, N. A. *Macromolecules* **1994**, *27*, 4084−4092.
(24) Manneville, P.; de Seze, L. In *Numerical Methods in the Study of Critical Phenomena*; Dora, J. D., Demongeot, J., Lacolle, B., Eds.; Springer-Verlag: Berlin, 1981; pp 116−124.
(25) Stockmayer, W. H. *J. Chem. Phys.* **1944**, *12*, 125−131.
(26) Boots, H. M. J. In *Integration of Fundamental Polymer Science and Technology*; Kleintjens, L., Lemstra, P., Eds.; Elsevier Appl. Sci.: London, 1986; pp 204−208.

(27) Boots, H.; Pandey, R. B. *Polym. Bull. (Berlin)* **1984**, *11*, 415−420.
(28) Simon, G. P.; Allen, P. E. E.; Bennett, D. J.; Williams, D. R. G.; Williams, E. H. *Macromolecules* **1989**, *22*, 3555−3561.
(29) Bowman, C. N.; Peppas, N. A. *J. Polym. Sci., Part A: Polym. Chem.* **1991**, *29*, 1575−1583.
(30) Herrmann, H.; Landau, D.; Stauffer, D. *Phys. Rev. Lett.* **1982**, *49*, 412−415.
(31) Bansil, R.; Herrmann, H. J.; Stauffer, D. *Macromolecules* **1984**, *17*, 998−1004.
(32) Bowman, C. N.; Peppas, N. A. *Chem. Eng. Sci.* **1992**, *47*, 1411−1419.
(33) Chiu, Y. Y.; Lee, L. J. *J. Polym. Sci., Part A* **1995**, *33*, 269−283.
(34) Anseth, K. S.; Bowman, C. N. *Chem. Eng. Sci.* **1994**, *49*, 2207−2217.
(35) Anseth, K. S.; Bowman, C. N. *J. Polym. Sci., Part B: Polym. Phys.* **1995**, *33*, 1769−1780.
(36) Sun, X.; Chiu, Y.; Lee, L. J. *Ind. Eng. Chem. Res.* **1997**, *36*, 1343−1351.
(37) Gillespie, D. *J. Comput. Phys.* **1976**, *22*, 403−434.
(38) Scappin, M.; Canu, P. *Chem. Eng. Sci.* **2001**, *56*, 5157−5175.
(39) Le Novere, N.; Shimizu, T. S. *Bioinformatics* **2001**, *17*, 575−576.
(40) Charnley, S. B. *Astrophys. J.* **1998**, *509*, L121−L124.
(41) Kurdikar, D. L.; Somvarsky, J.; Dusek, K.; Peppas, N. A. *Macromolecules* **1995**, *28*, 5910.
(42) Somvarsky, J.; Dusek, K. *Polym. Bull. (Berlin)* **1994**, *33*, 369−376.
(43) Somvarsky, J.; Dusek, K. *Polym. Bull. (Berlin)* **1994**, *33*, 377−384.
(44) Rankin, S. E.; Kasehagen, L. J.; McCormick, A. V.; Macosko, C. W. *Macromolecules* **2000**, *33*, 7639−7648.
(45) Even, J.; Bertault, M. *J. Chem. Phys.* **1999**, *110*, 1087−1096.
(46) Dooling, D. J.; Broadbelt, L. J. *Ind. Eng. Chem. Res.* **2001**, *40*, 522−529.
(47) Wang, H.; Xin, H. *Physica A* **1998**, *251*, 389−398.
(48) Wen, M.; Scriven, L. E.; McCormick, A. V. *Macromolecules*, in press.
(49) Stauffer, D.; Adler, J.; Aharnoy, A. *J. Phys. A: Math. Gen.* **1994**, *27*, L475−L480.
(50) Kurdikar, D. L.; Peppas, N. A. *Macromolecules* **1994**, *27*, 733−738.
(51) Akkermans, R. L. C. *J. Chem. Phys.* **1998**, *109*, 2929−2940.
(52) Odian, G. *Principles of Polymerization*, 3rd ed.; John Wiley & Sons: New York, 1992.
(53) Press, W. H.; Teukolsky, S. A.; Vetterling, W. T.; Flannery, B. P. *Numerical Recipes in Fortran: The Art of Scientific Computing*, 2nd ed.; Cambridge University Press: New York, 1992.
(54) Landin, D. T. Formation-Structure and Structure−Property Relationships during Vinyl-Divinyl Copolymerization. Ph.D. Thesis, University of Minnesota, 1985.
(55) Bansil, R.; Willings, M.; Herrmann, H. J. *J. Phys. A: Math. Gen.* **1986**, *19*, L1209−L1213.
(56) Jager, W. F.; Lungu, A.; Chen, D. Y.; Neckers, D. C. *Macromolecules* **1997**, *30*, 780−791.
(57) Chiu, Y. Y.; Lee, L. J. *J. Polym. Sci., Part A* **1995**, *33*, 257−267.
(58) Boots, H. M. J.; Kloosterboer, J. G.; van de Hei, G. M. M.; Pandey, R. B. *Br. Polym. J.* **1985**, *17*, 219−222.
(59) Anseth, K. S.; Anderson, K. J.; Bowman, C. N. *Macromol. Chem. Phys.* **1996**, *197*, 833−848.
(60) Kannurpatti, A. R.; Anseth, J. W.; Bowman, C. N. *Polymer* **1998**, *39*, 2507−2513.
(61) Dusek, K.; Somvarsky, J. *Polym. Int.* **1997**, *44*, 225−236.
(62) Matsumoto, A. *Adv. Polym. Sci.* **1995**, *123*, 41−80.
(63) Matsumoto, A. *Prog. Polym. Sci.* **2001**, *26*, 189−257.
(64) Zhu, S.; Tian, Y.; Hamielec, A. E.; Eaton, D. R. *Macromolecules* **1990**, *23*, 1144−1150.
(65) Allen, P.; Simon, G.; Williams, D.; Williams, E. *Macromolecules* **1989**, *22*, 809−816.
(66) Spevacek, J.; Dusek, K. *J. Polym. Sci., Polym. Phys. Ed.* **1980**, *18*, 2027−2035.
(67) Song, H. H.; Roe, R.-J. *Macromolecules* **1987**, *20*, 2723−2732.
(68) Mallamace, F.; Micali, N.; Vasi, C.; Bansil, R.; Pajevic, S.; Sciortino, F. *Prog. Colloid Polym. Sci.* **1992**, *89*, 77−81.
(69) Kannurpatti, A. R.; Lu, S.; Bowman, C. N. *Polym. Mater. Sci. Eng.* **1996**, *74*, 358−359.
(70) Kannurpatti, A. R.; Anderson, K. J.; Anseth, J. W.; Bowman, C. N. *J. Polym. Sci., Part B: Polym. Phys.* **1997**, *35*, 2297−2307.
(71) Jeffrey, K.; Pethrick, R. A. *Eur. Polym. J.* **1994**, *30*, 153−158.
(72) Jean, Y. C.; Deng, Q. *J. Polym. Sci., Part B* **1992**, *30*, 1359−1364.
(73) Liu, J.; Deng, Q.; Jean, Y. C. *Macromolecules* **1993**, *26*, 7149−7155.
(74) Anseth, K. S.; Rothenberg, M. D.; Bowman, C. N. *Macromolecules* **1994**, *27*, 2890−2892.
(75) Royal, J. S.; Victor, J. G.; Torkelson, J. M. *Macromolecules* **1992**, *25*, 729−734.

MA010308Q